

# Actively Tuned Plasmons on Elastomerically Driven Au Nanoparticle Dimers

Fumin Huang\* and Jeremy J. Baumberg

Nanophotonics Centre, Cavendish Laboratory, University of Cambridge, Cambridge, CB3 0HE, U.K.

**ABSTRACT** We demonstrate a novel way to actively tune surface plasmons by fabricating plasmonic nanostructures on stretchable elastomeric films. This allows reversible modification of the metal geometry on the nanometer scale. Using 100 nm scale Au nanoparticle dimers whose spacing is stretch-tuned reveals radically different spectral tuning than previously reported for sub-10-nm nanoparticles, but which can be explained by a revised interpretation of existing models. Tuning plasmons in this way offers a much more robust way than lithography to interrogate the physics of localized plasmons and has applications in optimized surface-enhanced luminescence and Raman scattering.

**KEYWORDS** Surface plasmon, elastomer, tunable, nanoparticle dimers, Raman scattering

Tuning the plasmonic coupling between metallic nanoparticles is highly desirable for many applications, for example, to develop ultrasensitive Raman and fluorescence sensors,<sup>1–3</sup> to design highly efficient optical antennas,<sup>4</sup> or to engineer the radiation properties of single emitters.<sup>5</sup> Although there have been many examples of investigating plasmonic nanostructures using arrays of lithographic patterns<sup>6–8</sup> or pairs of nanoparticles,<sup>9,10</sup> these approaches do not allow *active* tuning of the surface plasmons. More significantly, it is extremely hard to control nanostructure geometry on the 1 nm scale crucial for plasmonic resonances: a slight variation in particle shape, size, and interparticle separation can cause extreme modifications to the plasmonic resonance and atomic mobility of the relevant coinage metals leads to nanostructure aging. While active plasmon tuning has been demonstrated before, it is significantly limited by the approaches adopted, involving optical,<sup>12</sup> electronic,<sup>13</sup> ferroelectric,<sup>14</sup> and thermal<sup>15</sup> tuning mechanisms. An alternative approach is to fabricate plasmonic structures on mechanically tunable substrates, which has been demonstrated in only a few limited examples: in nanovoids,<sup>16</sup> gratings,<sup>17</sup> and plasmonic particle arrays.<sup>18</sup> In the latter two cases, the tuning controls optical-scale interference between emission from separate scatterers, while in the former case the continuous nature of the metal structure limited the mechanical tuning. Recently Tao et al.<sup>19</sup> reported using Langmuir–Blodgett techniques to assemble silver nanocrystals into close-packed two-dimensional arrays. Compressing these arrays (irreversibly) tunes the plasmonic coupling giving dramatic color changes but also demonstrates the need for techniques offering continuous and reversible tuning.

Here we report the active tuning of plasmons on a single Au nanoparticle dimer. Study of individual structures is crucial because sample inhomogeneities otherwise dominate the scattering spectra. An individual nanoparticle dimer is particularly interesting as it is the simplest geometry to study plasmonic coupling between nanoparticles, allowing improved understanding of plasmonic coupling at small scales. It is also extremely important for many applications since the local optical fields in the interstitial space between two nanoparticles can be strongly enhanced by several orders of magnitude under plasmonic resonant conditions, which is responsible for enhanced Raman and fluorescence signals as well as many other phenomena. The coupling between pairs of small nanoparticles has been extensively studied,<sup>6–10</sup> however, we reveal that scattering from slightly larger nanoparticles remains relatively unknown still. Here we demonstrate active tuning of the coupling between individual pairs of Au nanospheres (radius  $a = 125$  nm) deposited on stretchable elastomeric films. The measured dark-field (DF) scattering spectra at different stretching distances show intriguingly different behavior from those reported on small nanoparticles ( $a \ll \lambda$ )<sup>6–10</sup> and are clearly anisotropic with polarization. The experimental results are found to be in good agreement with theoretical simulations and demonstrate the need to update the conventional intuition.

To clarify the effect of particle size, we calculate the total elastic scattering cross sections of single Au nanospheres with increasing size (Figure 1a), based on a boundary element method.<sup>20</sup> For small spheres ( $a \ll \lambda$ ), the scattering spectra are primarily dominated by a dipole mode (Figure 1a,  $a = 10–100$  nm). When the sphere size is much smaller than the wavelength of light, retardation effects can be ignored and thus the induced dipole moment of the sphere illuminated by a uniform plane wave is given by a quasi-static approximation,  $p \propto a^3((\epsilon - 1)/(\epsilon + 2))$ , where  $a$  is the sphere radius and  $\epsilon$  is its dielectric function (in air). The

\* To whom correspondence should be addressed. fh281@cam.ac.uk.

Received for review: 02/03/2010

Published on Web: 00/00/0000

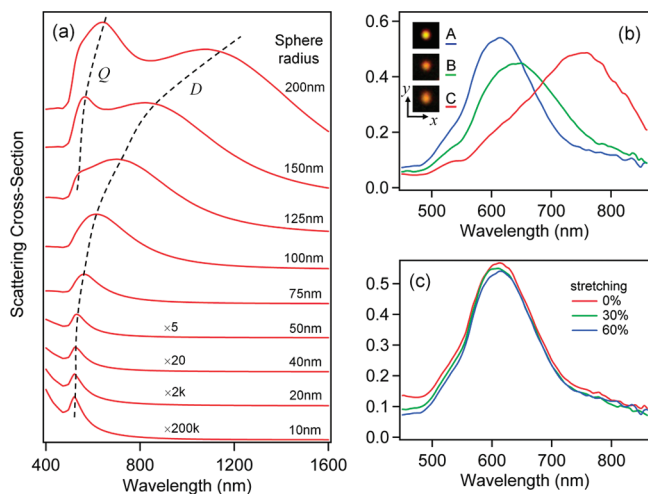


**FIGURE 1.** (a) Calculated total elastic scattering cross sections of single Au nanospheres with increasing radii  $a$ . (b) Measured dark-field scattering spectra of single Au nanoparticles of different sizes. (inset) Dark-field microscope images of the nanoparticles, image size  $2.5 \times 2.5 \mu\text{m}$ . (c) Measured dark-field scattering spectra of particle A when the elastomeric film is stretched.

resonant condition is determined by minimizing the denominator, which gives a wavelength of 520 nm for small Au spheres. When the sphere size increases, retardation effects become significant. As a consequence higher order multiple modes appear (starting with the quadrupole mode,  $Q$ ), while the dipole mode ( $D$ ) red shifts to longer wavelengths in Figure 1a.

This dependence can be clearly seen in the measured dark-field scattering spectra of single Au nanospheres with different sizes (Figure 1b). The Au nanospheres<sup>11</sup> (diameter 250 nm) were sparsely deposited on an transparent acrylic elastomeric film by a drop-cast method. Dark-field scattering spectra were measured using a modified confocally arranged optical microscope using incident incandescent light while scattering was collected with a high numerical aperture objective (NA 0.8) and normalized to the incident spectrum. Scanning electron microscope (SEM) images confirm that the size of most nanoparticles is around 250 nm (Supporting Information, Figure S1) with <5% size variation measured and some facetting; however these do not strongly affect the results here for separations greater than the facet scale. Figure 1b shows the measured dark-field scattering spectra of three nanoparticles of different sizes (Figure 1b, inset), which clearly show a red shift in the peak position of the spectra with increasing particle size, consistent with theoretical calculations. Most particles are similar to particle A, while particle C is an exceptionally big one. The shape of the spectra are not exactly the same as those of simulations, which will be discussed later in this Letter.

To confirm that nanoparticle morphology and shape is not affected by stretching the underlying substrate, the dark-field scattering spectra of particle A in Figure 1b is measured as the elastomer film is stretched (Figure 1c). These spectra are almost unchanged during stretching, indicating that the

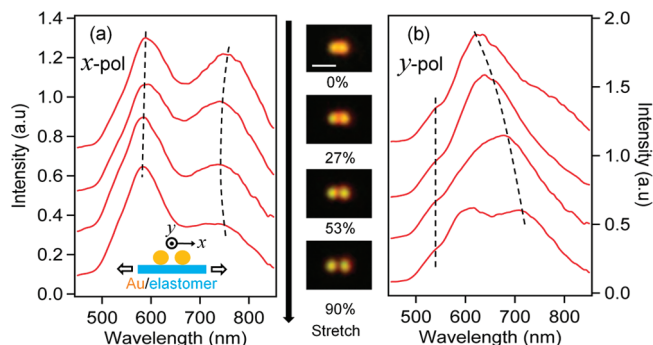


**FIGURE 2.** Measured dark-field scattering spectra of a single Au nanoparticle dimer deposited on stretchable elastomeric film. From top to bottom, the film is stretched by 0%, 27%, 53%, and 90%. Incident light is polarized along (a) the dimer axis ( $x$  direction, as in lower schematic) and (b) perpendicular to the dimer axis ( $y$  direction). (middle) Dark-field microscope images of the dimer at different stretching distances; scale bar is  $1 \mu\text{m}$ .

particle geometry is not modified. The spectra in Figure 1b,c are measured with incident light polarized along the  $x$  direction indicated; however, the spectra with light polarized along the  $y$  direction (not shown) are almost identical, indicating that the shapes of these particles are close to spheres. These data also confirm that the stretch-induced change in refractive index of the substrate does not impact the plasmon coupling, since the optical field is not concentrated at this interface.

A single pair of Au nanospheres deposited on the elastomeric substrate is now selected, and their dark-field scattering spectra are measured (Figure 2). Stretching the elastomeric film (as in Figure 2a, inset) allows active tuning of the interparticle gaps without deforming the particle geometries, such as their size or shape. The incident light is polarized both parallel to the axis of the dimer ( $x$  direction, Figure 2a) and perpendicular to the dimer axis ( $y$  direction, Figure 2b). In the former case ( $x$ ) the spectra exhibit two resonant scattering peaks. The short wavelength peak remains almost independent of the interparticle gap while the longer wavelength peak is slightly blue-shifted and the peak intensity decreases, as the interparticle gap increases. However when the perpendicular polarization is used ( $y$ , Figure 2b), the scattering spectra are significantly different: the major peak obviously *red shifts* as the interparticle gap increases. They are also much stronger in intensity than those excited under  $x$  polarization. The microscope images of the two particles at increasing stretching distances (Figure 2, middle) clearly show the widening interparticle separation. These spectral changes are repeatable as the elastomeric film is relaxed back and can be cycled, clearly demonstrating effective mechanical tuning of localized plasmons and their resonant fields.

Such results are dramatically different from those reported from pairs of small nanoparticles.<sup>6–10</sup> For dimers of two small nanoparticles, usually the resonant peaks of the scattering spectra red shift with decreasing gaps when the incident light is polarized along the dimer axis with no

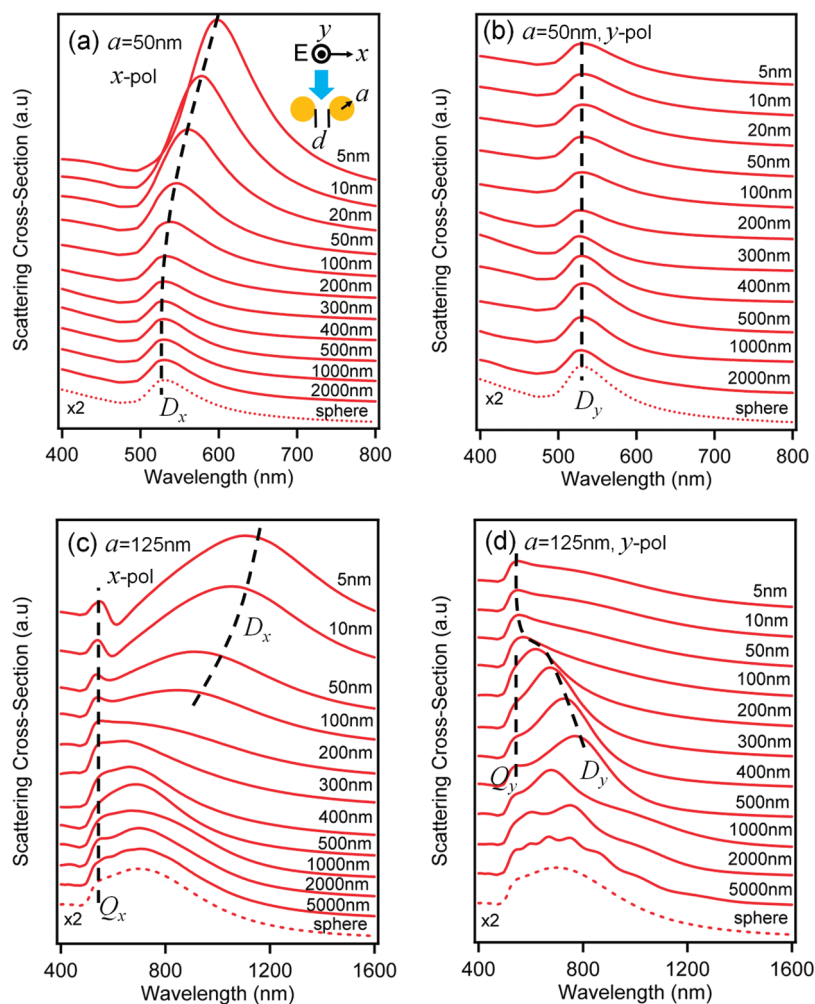


FIGURE 3. Calculated total elastic scattering cross sections of Au sphere dimer, for geometry as inset in (a). Sphere radius (a, b)  $a = 50$  nm, (c, d)  $a = 125$  nm. Incident polarization along  $x$  (a, c) and  $y$  (b, d) directions. Lower dashed spectra are for single spheres (multiplied by 2).

change for perpendicular polarizations. This behavior is reproduced theoretically by the total elastic scattering cross sections of a Au sphere dimer (radius  $a = 50$  nm) under (a) parallel and (b) perpendicular polarization illumination (Figure 3a,b), for the configuration depicted (inset). The typical behavior of dimers of small nanoparticles is seen, with *single* scattering peaks which *red shift* for decreasing interparticle gap in  $x$  polarization but show no change for  $y$  polarization.

However for large particle dimers, the situation is significantly different. In Figure 3(c,d) we show the calculated total elastic scattering cross sections of a pair of Au spheres with radius of 125 nm, under (c) parallel and (d) perpendicular polarizations which reveal more complicated spectra quite different from those of smaller nanoparticles. These spectra can be discussed within three regions corresponding to different interparticle separations.

(i) Close distances ( $d < a$ ): With polarization parallel to the dimer axis (Figure 3c), at close distances the dipole modes ( $D_x$ ) red shift as the interparticle gap decreases, similar to the case of small nanoparticle dimers. An additional peak

also appears at short wavelength due to the quadrupole mode ( $Q_x$ ), which is unaffected by morphology. When the polarization is perpendicular to the dimer axis (Figure 3d), the scattering spectra vary little at close distances (from  $d = 5-100$  nm). However there is a significant difference from small particle dimers (which show spectra almost identical to those of single spheres under  $y$  polarization) indicating that the coupling between two small nanoparticles under perpendicular excitation is weak. For large sphere dimers the spectra are modified from that of single spheres, indicating strong coupling between the two spheres even under  $y$  polarization.

(ii) Medium distances ( $d$  comparable to  $a$ ): Dramatic changes emerge for gaps comparable to the sphere size, a range here spanning 100–500 nm in Figure 3c,d. In this region, there is very strong coupling under  $y$  polarization, which is even stronger than under  $x$  polarization excitation, an unusual phenomenon not seen in small particle dimers. In Figure 3d a strong resonant peak red shifts away from the largely unaffected quadrupole mode ( $Q_y$ ) as the gap

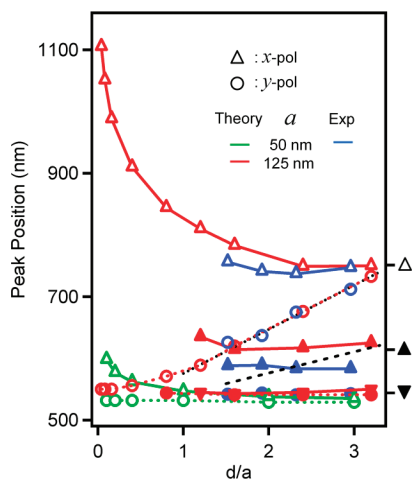


FIGURE 4. Plasmon resonance positions as a function of interparticle gap (normalized to particle radius), for  $x$ -pol (open and solid triangles) and  $y$ -pol (open and solid circles). Theory for  $a = 125$  nm (red) and  $a = 50$  nm (green), experiment (blue). Single sphere  $a = 125$  nm (black triangle). Linear fits for  $y$ -pol on dimer with  $a = 125$  nm (dotted) or  $a = 100$  nm (dashed) spheres.

increases. Under  $x$  polarization the coupling is weak and the spectra are similar to that of single sphere (dashed line), apart from the long tail in the longer wavelength region. As the particle gap increases, the longer-wavelength tail diminishes, and the spectra tend to those of single spheres.

(iii) Large distances ( $d \gg a$ ): Here for  $d > 5000$  nm, the scattering spectra in both polarizations resemble the sum of two individual spheres (dashed spectra), apart from extra interference fringes, because the coupling between the two particles at such distances is very weak.

To further discuss the simulation results shown in Figure 3, we plot in Figure 4 the peak positions of the modes as a function of the interparticle gap,  $d$  (normalized to the sphere radius  $a$ ). For smaller spheres ( $a = 50$  nm), under  $x$  polarization (green triangle) the peak position red shifts exponentially with decreasing gaps at close distances, while it is almost unchanged for  $y$  polarization (green circle). For large particles ( $a = 125$  nm), under perpendicular polarization, the peak position (red circle) was mostly unchanged at close distances, then red shifts linearly with increasing interparticle gap  $d$ . The quadrupole modes (red, filled circles) remain mostly unchanged. For  $x$  polarization, at close distances, the dipole mode red shifts exponentially with decreasing interparticle gap, similar to that of dimers of small nanoparticles. The strong dipole peaks at close distances weaken significantly in intensity as the gap increases, making determination of the peak positions more difficult. In this medium distance region ( $150 < d < 500$  nm), the spectra can be best fit with three Gaussian functions. The results reveal an almost unchanged quadrupole mode around 540 nm (solid red down triangle), and two other modes with longer wavelengths (red solid and open up triangle). For comparison, we also similarly fit the single sphere ( $a = 125$  nm) spectrum giving the black triangles on the right side of Figure

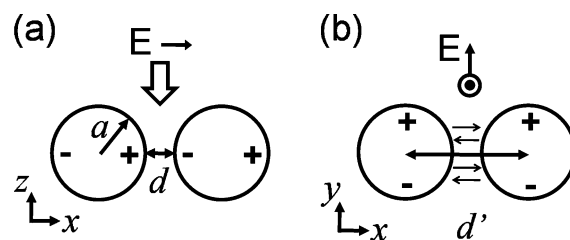


FIGURE 5. Schematic charge distributions on a pair of spheres under broadside illumination with (a) parallel polarization along the dimer axis ( $x$ -pol) and (b) transverse polarization perpendicular to the dimer axis ( $y$ -pol). In the former case, the charges accumulated at the two surfaces facing each other form a strong electric dipole, which dominates the scattering spectra at close distances, as shown in parts a and c of Figure 3. In the latter case, the charges are mostly accumulated on the surfaces perpendicular to the dimer axis; which is at least at the order of sphere diameter. In the case of large spheres, they scatter strongly along the dimer axis (as arrows indicate), therefore resulting in interference fringes as interparticle distance increases, as shown in Figure 3d.

4. Only the longest wavelength dipole mode red shifts as the gap decreases, and at large distance the modes tend to those of the single sphere.

To qualitatively interpret these results, we show schematic diagrams of the charge distributions on the dimer under different polarizations (Figure 5), which are supported by numerical simulations. Under  $x$  polarization (Figure 5a), at very close distances, large charge densities with opposite signs accumulate at the sphere surfaces near the gap facing each other, forming a strong dipole which dominates the scattering spectra. This dipole sensitively depends on the interparticle gap, resulting in a quasi-exponential red shift of the dipole mode as the dimer gap decreases. At medium distances ( $d = 200$ – $500$  nm), the coupling between the two spheres is weak, as the dipoles of the two spheres point parallel to each other and radiate weakly in that direction. Under  $y$  polarization (Figure 5b), most charges are distributed at the top and bottom surfaces of the spheres (simulation results indicate a slight sideways shift away from the upper and lower points as a result of repulsive forces between the two spheres). Considering the dipoles as located at the sphere centers implies that the dipole interaction distances ( $d'$ ) are on the order of the sphere diameter; therefore a small change of interparticle gap at close distances does not induce significant changes to the scattering spectra, as found in Figure 3d. As the two dipoles are coaligned perpendicular to the long axis of the dimer, they radiate strongly in the direction along the dimer axis, therefore strongly coupling to each other through multiple scattering processes.<sup>21</sup> This phenomenon is not observed on small particles, because for small spheres, the scattering cross sections are so weak they are negligible compared to the incident field at such distances. However as particle size increases, the scattering strength increases significantly (the scattering intensity of the 125 nm sphere in Figure 1a is 20 times that of the 50 nm sphere). As it becomes comparable to the incident field, the multiple-scattering process between

the two spheres plays an important role, significantly modulating the scattering spectrum. The spectral positions of the major scattering peaks (Figure 4, red circle) as a function of interparticle gap,  $d$ , can be well fit with a linear relationship indicative of interference effects,  $\lambda = 0.56d + 504$  nm (black dotted line), similar to a Fabry–Perot cavity. As the gap further increases, more interference fringes appear (Figure 3d). We note that these interference features are rather robust and insensitive to the illumination or detection conditions.

Comparing experimental (Figure 2) and simulation results (Figure 3c,d) shows good agreement where the gaps between the two Au nanoparticles are in the range 190–370 nm. Larger experimental dimer separations were determined from optical images, as the center-to-center distances were clearly resolved (see middle images Figure 2). Confirmation of the linear dependence of separation on applied strain then allowed us to calibrate gaps that could not be directly optically resolved. Both experiment and theory show strong polarization-anisotropy with  $y$ -pol stronger than the  $x$ -pol scattering. Under  $y$ -pol, both show the peak positions (blue and red circles) red shift linearly with increasing interparticle gaps. Quadrupole modes around 540 nm seen in both remain mostly unchanged with interparticle gap. Under  $x$ -pol, both show the long wavelength dipole mode shifts with gap separation (blue triangle). This strongly supports our conclusions of effective stretch tuning of these dimers.

The remaining discrepancies between measured spectra and simulations can be tracked down to more complicated theoretical angular scattering than previously reported, depending not only on the incident light direction and polarization but also on the precise collection angles. In simulations here incident plane waves are used and the scattered light is collected through the full  $4\pi$  solid angle, while in experiments illumination occurs through a dark-field objective and light is collected in a backscattering configuration within limited collection angles. While a more detailed investigation will be reported elsewhere, this is already seen in a recent paper on single nanoparticles,<sup>22</sup> and dimers exacerbate the situation greatly.

Overall a straightforward picture of the coupling between two spheres is produced: the scattering spectrum of a dimer follows the scattering spectrum of a single sphere modulated by the coupling effect between the two spheres, an analogue to double slit interference. At close distances the coupling effect is so strong that the spectra are significantly modified, while as the gap increases coupling weakens and the dimer spectrum recovers to the single sphere case. The combination of interferometric coupling and resonance shifts leads to multiple peaks in the scattering spectra which can often appear asymmetrically broadened. Sometimes experiments resolve clear multiple peaks (Figure 2b,  $y$ -pol, 90% extension) not present in simulations, possibly due to erroneously broad single sphere scattering peaks.<sup>22</sup> The good agreement

found here between theory and experiment is indeed rather sensitive to the precise size of the nanoparticles, so that  $y$ -pol scattering spectra for  $a = 100$  nm spheres give very different results (Figure 4, black dashed line). This suggests scanning dimer separations is an effective tool for distinguishing nanoparticle sizes in situ. We estimate sphere sizes accurate to within 10 nm, with strain control of 1% allowing nanometer-scale precision when optimized.

In conclusion, we report a novel way to actively tune the plasmonic properties of nanostructures, by fabricating metal–elastomer nanostructures. Mechanically stretching the elastomeric films allows real-time tuning of the interparticle gaps without deforming the actual particle structure. We demonstrate active plasmon tuning of individual Au nanoparticle dimers and thus reveal for sizes just above 100 nm dramatically different behaviors from those of small nanoparticles. This technique may be further exploited for applications in a wide variety of areas. Though the reported interparticle distances here are in the range of hundred nanometers, this elastomeric method can also be used to tune interparticle separations at very short distances, therefore maximally optimizing the field enhancements at the interstitial spaces of two nanoparticles, which is essential for producing extremely high surface-enhanced Raman scattering signals for the detection of single molecules.<sup>23</sup> For example, one can fabricate bowtie or dimer nanostructures first by lithographic methods and then transfer them onto elastomeric films. Alternatively one can use molecular linkers to bind two particles together with a weak bond which can be broken by stretching, and thus allow fine-tuning of interparticle distances (experiments in progress).

**Acknowledgment.** This work is supported by EPSRC Grants EP/G060649/1, EP/H007024/1, and EP/F059396/1.

**Supporting Information Available.** SEM images of a single Au nanoparticle and a dimer of two Au nanoparticles. This material is available free of charge via the Internet at <http://pubs.acs.org>.

## REFERENCES AND NOTES

- (1) Anker, J. N.; Hall, W. P.; Lyandres, O.; Shah, N. C.; Zhao, J.; Van Duyne, R. P. *Nat. Mater.* **2008**, *7*, 442–453.
- (2) Kinkhabwala, A.; Yu, Z.; Fan, S.; Avlasevich, Y.; Mullen, K.; Moerner, W. E. *Nat. Photonics* **2009**, *3*, 654–657.
- (3) Lim, D. K.; Jeon, K. S.; Kim, H. M.; Nam, J. M.; Suh, Y. D. *Nat. Mater.* **2010**, *9*, 60–67.
- (4) Alu, A.; Engheta, N. *Nat. Photonics* **2008**, *2*, 307–310.
- (5) Farahani, J. N.; Pohl, D. W.; Eisler, H.-J.; Hecht, B. *Phys. Rev. Lett.* **2005**, *95*, No. 017402.
- (6) Su, K.-H.; Wei, Q.-H.; Zhang, X.; Mock, J. J.; Smith, D. R.; Schultz, S. *Nano Lett.* **2003**, *3*, 1087–1090.
- (7) Gunnarsson, L.; Rindzevicius, T.; Prikulis, J.; Kasemo, B.; Kall, M.; Zou, S.; Schatz, G. C. *J. Phys. Chem. B* **2005**, *109*, 1079–1087.
- (8) Jain, P. K.; Huang, W.; El-Sayed, M. A. *Nano Lett.* **2007**, *7*, 2080–2088.
- (9) Lassiter, J. B.; Aizpurua, J.; Hernandez, L. I.; Brandl, D. W.; Romero, I.; Lal, S.; Hafner, J. H.; Nordlander, P.; Halas, N. J. *Nano Lett.* **2008**, *8*, 1212–1218.
- (10) Reinhard, B. M.; Siu, M.; Agarwal, H.; Alivisatos, A. H.; Liphardt, J. *Nano Lett.* **2005**, *5*, 2246–2252.

- (11) EM.GC250, British Biocell International .
- (12) Krasavin, A. V.; Zayats, A. V.; Zheludev, N. I. *J. Opt. A* **2005**, *7*, S85–S89.
- (13) Berthelot, J.; Bouhelier, A.; Huang, C.; Margueritat, J.; Colas-des-Francis, G.; Finot, E.; Weeber, J.-C.; Dereux, A.; Kostcheev, S.; El Ahrach, H. L.; Baudrion, A.-L.; Plain, J.; Bachelot, R.; Royer, P.; Wiederrecht, G. P. *Nano Lett.* **2009**, *9*, 3914–3921.
- (14) Chen, H. L.; Hsieh, K. C.; Lin, C. H.; Chen, S. H. *Nanotechnology* **2008**, *19*, 435304.
- (15) Xu, G.; Chen, Y.; Tazawa, M.; Jin, P. *J. Phys. Chem. B* **2006**, *110*, 2051–2056.
- (16) Cole, R. M.; Mahajan, S.; Baumberg, J. J. *Appl. Phys. Lett.* **2009**, *95*, 154103.
- (17) Olcum, S.; Kocabas, A.; Ertas, G.; Atalar, A.; Aydinli, A. *Opt. Express* **2009**, *17*, 8542–8547.
- (18) Malynych, S.; Chumanov, G. J. *Am. Chem. Soc.* **2003**, *125*, 2896–2898.
- (19) Tao, A.; Sinsersuksakul, P.; Yang, P. *Nat. Nanotechnol.* **2007**, *2*, 435–440.
- (20) Garcia de Abajo, F. J.; Howie, A. *Phys. Rev. B* **2002**, *65*, 115418.
- (21) Bruning, J. H. *IEEE Trans. Antennas Propag.* **1971**, *19*, 378–390.
- (22) Knight, M. W.; Fan, J.; Capasso, F.; Halas, N. J. *Opt. Express* **2010**, *18*, 2579–2587.
- (23) Xu, H.; Aizpurua, J.; Kall, M.; Apell, P. *Phys. Rev. B* **2002**, *62*, 4318.